Journal of Materials Chemistry B

Surface engineering of porous silicon to optimise therapeutic antibody loading and release

Journal:	*Journal of Materials Chemistry B*
Manuscript ID:	TB-ART-03-2015-000397
Article Type:	Paper
Date Submitted by the Author:	02-Mar-2015

Complete List of Authors:	McInnes, Steven; Univrseity of South Australia, Mawson Institute Turner, Chris; University of South Australia, Mawson Institute Al-Bataineh, Sameer; University of South Australia, Mawson Institute Airaghi Leccardi, Marta; ETH Zurich, Department of Materials; University of South Australia, Mawson Institute Irani, Yazad; Flinders University, Department of Ophthalmology Williams, Keryn; Flinders University, Department of Ophthalmology Cowin, Allison; University of South Australia, Mawson Institute Voelcker, Nicolas; University of South Australia, Mawson Institute

Journal of Materials Chemistry B RSCPublishing

ARTICLE

Surface engineering of porous silicon to optimise therapeutic antibody loading and release†

Cite this: DOI: 10.1039/x0xx00000x

Steven J. P. McInnes,[a] Chris T. Turner,[b] Sameer A. Al-Bataineh,[b] Marta J. I. Airaghi Leccardi,[a] Yazad Irani,[c] Keryn A. Williams,[c] Allison J. Cowin[b] and Nicolas H. Voelcker[a*]

Received ooth January 2015,
Accepted ooth January 2015

DOI: 10.1039/x0xx00000x

www.rsc.org/

The proinflammatory cytokine, tumor necrosis factor-α (TNF-α), is elevated in several diseases such as uveitis, rheumatoid arthritis and non-healing chronic wounds. Adding Infliximab, a chimeric IgG1 monoclonal antibody raised against TNF- α, to chronic wound fluid can neutralise human TNF-α, thereby providing a potential therapeutic option for chronic wound healing. However, to avoid the need for repeated application in a clinical setting, and protect the therapeutic antibody from the hostile environment of the wound, suitable delivery vehicles are required. Porous silicon (pSi) is a biodegradable high surface area material commonly used for drug delivery applications. In this study, the use of pSi microparticles (pSi MPs) for the controlled release of Infliximab to disease environments, such as chronic wounds, is demonstrated. Surface chemistry and pore parameters for Infliximab loading are first optimised in pSi films and loading conditions are transferred to pSi MPs. Loading regimens exceeding 60 µg of Infliximab per mg of pSi are achieved. Infliximab is released with zero-order release kinetics over the course of 8 days. Critically, the released antibody remains functional and is able to neutralise TNF-α over a weeklong timeframe; suitable for a clinical application in chronic wound therapy.

Introduction

Protein therapeutics are becoming more and more prevalent in the treatment of a variety of diseases and medical conditions.[1,2] However, as proteins are relatively unstable and readily degraded, there is a need to develop alternative effective delivery systems.[3] These delivery systems need to protect the protein from degradation by proteases and hydrolytic conditions whilst also being completely biodegradable naturally in the body after implantation or injection.[3]

Porous silicon (pSi) is a biomaterial that is now under intense focus as it has several unique properties that make it very attractive for use in a wide variety of *in vivo* and *ex vivo* applications.[4,5] Bulk crystalline silicon is converted into the high surface area and biocompatible pSi by means of anodisation in hydrofluoric acid (HF) solution. A broad range of porous structures can be generated by altering the wafer resistivity, HF concentrations and the applied current densities. The pore size can be tuned in diameter from a few nanometers to a few microns achieving surface areas of up to 800 m^2/g.[3,6] pSi degradation is tunable, from days to months,[3,7,8] depending on the pore size and chemistry and produces non-toxic silicic acid.[6,9-11] pSi has demonstrated *in vivo* biocompatiblity in the subconjuctival space of rats[12] and when injected into the vitreous of rabbit eyes.[13] Bimbo *et al.* have also demonstrated the biodistribution of pSi nanoparticles (NPs) administered via oral, subcutaneous and intravenous administration and shown that the pSi NPs do not induce toxicity or inflammatory responses whilst displaying excellent *in vivo* stability in rats.[14] *Ex vivo* applications include optical biosensors that capitalise on the unique optical and photonic properties of the material and have been exploited in the fields of immunology,[15] cancer diagnostics,[16] chronic wound healing[17,18] and infectious diseases.[19] The ability of pSi to store and release various payloads of small molecular, oligonucleotide or even protein therapeutics has also been demonstrated.[20-22]

Immediately after fabrication, pSi is hydride-terminated and degrades within minutes when immersed in neutral aqueous medium. However, the surface chemistry of pSi can be easily modified by techniques such as oxidation, silanisation, hydrosilylation, hydrocarbonisation and electrografting in order to impart varying degrees of stability to the material in addition to introducing functional groups.[23-26] Certain surface modifications including thermal hydrocarbonisation render pSi stable even in harsh conditions such as exposure to strong aqueous bases.[27] The ability of pSi to degrade into non-toxic silicic acid upon exposure to physiological conditions is a key advantage over other biomaterials.[28] The choice of surface chemistry also plays an important role in the ability to load different drugs and must therefore be chosen carefully.[20,29] A range of *in vivo* and *in vitro* studies have demonstrated the biocompatibility of surface-modified pSi.[11,28,30,31] We recently demonstrated composite pSi and poly(ε-caprolactone) (PCL) membranes can be implanted into the subconjunctival space of rats.[32] These membranes did not erode or cause inflammatory responses in the tissue surrounding the implant and there was also no evidence of vascularisation.

pSi is being exploited for applications in drug delivery including in several preclinical and clinical settings.[12,33,34] A particularly suitable format of pSi for drug delivery are pSi microparticles (pSi MPs) that are fabricated to the desired size from "free-standing" membranes of pSi by sonication[35-38] or other mechanical forces, such as ball milling.[39] Given their fabrication from pSi films, those MPs have a characteristic plate shape. The Sailor laboratory has developed pSi MPs suitable for injection into the vitreous humor,[13] has shown intravitreal drug release for up to 6 months[33,40] and the ability to tune drug release by varying the pore size[41] or polymer encapsulation of the pSi MPs.[42] They have also extensively studied how the pSi dissolution by-products are cleared from the vitreous humor after injection of pSi MPs.[43]

Receptor proteins, including antibodies, can be both electrostatically bound or conjugated to pSi MPs or NPs for targeting[44,45] or biosensing[15,46] applications employing various chemistries such as thermal oxidation[46], amino-terminated silanes[47], or using semicarbazide[44], EDC/NHS[48] or click[49] chemistries. But very few examples exist in the literature describing the release of therapeutic proteins from pSi for therapeutic applications. One early example was performed by Foraker *et al.*[50] who used micromachined pSi particles to deliver insulin across intestinal Caco-2 cell monolayers. They found that the flux of insulin from the pSi particles was nearly 10 times higher than from insulin in solution and 100 times higher when permeation-enhancing chemicals were omitted in that solution. Likewise, Wu and Sailor have used a polymeric chitosan-based hydrogel to cap the top of pSi films and demonstrate controlled release of insulin from the underlying porous structure in a switchable pH dependent fashion.[51] In 2007, Prestidge *et al.*[52] used pSi powders to load and release papain, a model hydrophilic protein. It was observed that the powders, anodised and stain-etched, used in this study varied in surface chemistry, which subsequently affected the loading and burst release of the enzyme from the material. More recently, Andrew *et al.*[21] loaded a thermally oxidised pSi film with Avastin, a monoclonal antibody, and demonstrated a sustained release of 98% of active antibody after 1 month, but the authors did not translate this system to a fully degradable pSi MP format. The retention of the active form of the protein released from pSi MPs and NPs has also been demonstrated by other groups[53] emphasising the careful choice of surface chemistry to minimise possible denaturation.[54]

Infliximab is a chimeric IgG1 monoclonal antibody raised against tumor necrosis factor-α (TNF-α). This antibody is clinically approved to treat Crohn's disease[55] and rheumatoid arthritis.[56] Infliximab functions by neutralising the function of TNF-α. Infliximab has also been studied for the treatment of psoriasis[57,58], ulcerative colitis,[59,60] pyoderma gangrenosum,[61] chronic venous ulcers[62] and uveitis.[63] Non-healing chronic wounds including venous leg ulcers affect 1 – 2% of the population in developed countries and place a significant burden on the community, estimated to cost $15 billion dollars per year worldwide.[64] TNF-α has been demonstrated to be elevated in venous leg ulcers and Infliximab has proven successful in reducing TNF-α levels.[62] Uveitis, also an inflammatory condition, occurs in the uveal tract and is responsible for 10% of visual loss in developing nations.[65] Typical treatment is with topical and oral glucocorticosteroids and often patients receiving this treatment display significant side effects and insufficient therapeutic responses. Topically applied Infliximab has performed well in the reduction of scarring on the ocular surface in a mouse ocular surface scarring model.[63]

However, side effects of the systemic delivery of high-dose anti-TNF-α agents, including Infliximab and Etanercept, include drug-induced lupus[66] and treatment must be discontinued in these cases. Hence, the development of better delivery systems for anti-TNF-α, particularly those that can sustain low-dose release over a prolonged timespan, could prove beneficial for patient well-being and continual treatment. Indeed, previous studies have shown that the topical application of 10 mg/mL Infliximab as a solution or gel and covered with an adhesive bandage could reduce ulcer healing time to 8 weeks in approximately 30% of cases, while the other 70% of ulcers treated had healed significantly, showing a 75% reduction in size.[67] Similarly, the one off implantation or injection of a sustained drug delivery for Infliximab to the cornea and anterior segment may prove a safe and effective way to reduce the number of treatments required for anterior uveitis, hence improving patient care.

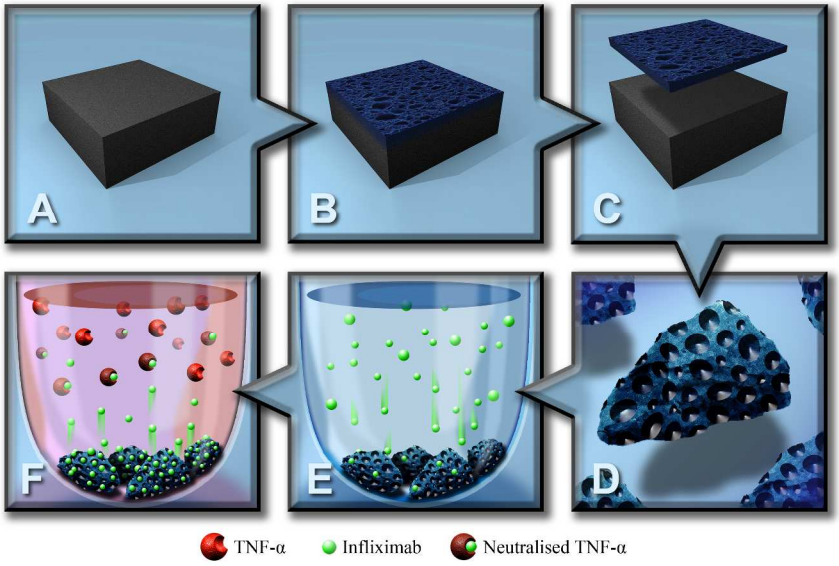

Scheme 1: (A) Crystalline silicon wafer prior to (B) electrochemical anodization to produce a pSi film. The film is then removed from the crystalline substrate via an electropolishing etch (C). The resulting free-standing pSi film is sonicated to generate pSi microparticles (MPs) which are subsequently oxidised at 400 °C and then loaded with the therapeutic antibody Infliximab (E). The Infliximab is released from the pSi and neutralizes TNF-α (F).

The current study aims to demonstrate the versatility of pSi as a reservoir for Infliximab delivery in both *in vivo* and *ex vivo* applications. pSi films with different pore size were prepared by electrochemical etching and thermally oxidised at a range of temperatures. The optimal etching conditions found for the films were then transferred to pSi MPs, which are fully degradable and, in contrast to pSi films, can be used for implantation or injection. pSi MPs were immersed in the antibody solution, allowing the positively

charged protein to penetrate into the pores by electrostatic attraction with the negatively charged surface. Antibody loading was quantified using interferometric reflectance spectroscopy and UV-Vis spectroscopy. Infliximab released from pSi MPs remained active and was able to neutralise TNF-α (Scheme 1), potentially providing an improved therapeutic delivery system for the treatment of chronic wounds and ocular conditions such as uveitis.

Experimental Details

Chemicals. Hydrofluoric acid (HF) 48% (Merck), dichloromethane (CH_2Cl_2, Labserv, analytical grade, 99.5%), methanol (Merck, analytical grade, 99.5%), acetone (Ajax, analytical grade, 99.5%), and ethanol (Ajax, absolute, 100%) were used without further purification. N,N-dimethylformamide (DMF, EMD Chemicals, Belgium) was purified via standard laboratory protocols including drying over $MgSO_4$ followed by distillation at reduced pressure.[68] Milli-Q water was obtained from an Advantage A10 water purification system provided by Merck Millipore (water resistivity of 18.2 MΩcm at 25 °C, TOC < 5 ppb). Phosphate buffered saline (PBS) solution was prepared by dissolving one PBS tablet (Sigma) in 200 mL of MilliQ water, giving a pH of 7.4.

Infliximab (Remicade®) powder was purchased from Janssen, Australia. Each vial contains 100 mg of Infliximab, 6.1 mg of sodium phosphate dibasic dehydrate, 2.2 mg of sodium phosphate monobasic monohydrate, 500 mg of sucrose and 0.5 mg of polysorbate 80. The undiluted Infliximab powder was stored at 4 °C. Before use the Infliximab powder was diluted to 1 mg/mL with MilliQ water (10 mL).

pSi film preparation. Si wafers (p-type boron doped with a resistivity range of 0.00055 - 0.001 Ωcm and a <100> crystal orientation) were cut in 3 - 4 cm^2 pieces, washed with high purity ethanol (Ajax, absolute, 100%) and placed into a Teflon cell, between two electrodes (a platinum mesh as cathode and an aluminum foil as anode for the back contact of Si). The exposed surface area was 1.767 cm^2 and the distance between the silicon and the Pt cathode was approximately 1.5 cm. A Keithley 2425 100 W Source Meter was used for anodisation. Etching current and time were controlled by a custom written Labview 8.2 computer program. Polished silicon wafers (CZ process, diameter of 76.2 mm and thickness between 475 - 525 μm) were provided by Siltronix. The wafer pieces were etched in a 3:1 HF:ethanol (v/v) solution. One sacrificial etching step was carried out at 200 mA (113 mA/cm^2) for 15 s and the freshly etched surface was washed with ethanol before treatment with 1 N sodium hydroxide for 1 min. The silicon surface was washed again with MilliQ water and ethanol and dried under nitrogen gas. The second etching process was performed with etching current densities ranging from 150 to 233 mA/cm^2 and etching times of 15 to 291 s. After etching, washes were performed with ethanol and dichloromethane and dried with nitrogen gas.

pSi MP preparation. Microparticles were fabricated from p-type Si wafers (boron-doped, resistivity < 0.001 Ωcm, <100>) supplied by Virginia Semiconductors (Fredericksburg, VA, USA). The wafer was anodised in an 18 cm^2 etching cell in 3:1 HF:ethanol (v/v) solution with a current density of 222 mA/cm^2 for 4 min, and then electropolished for 30 s at 500 mA/cm^2. Then, 20 min of sonication was performed (S30H Elmasonic, 280 W, Elma) to fracture the pSi membrane into MPs. The pSi MP suspension was filtered, washed with ethanol and dichloromethane before drying to completeness.

Gravimetric analysis. The porosity of pSi was determined by weight measurements. To do this, the wafer is weighed before etching (m_1), after etching (m_2) and after the porous layer is dissolved from the bulk Si, with NaOH (m_3). These three values can then be used to calculate the porosity using the following equation [5]:

$$\text{Porosity (\%)} = (m_1 - m_2)/(m_1 - m_3) \qquad \text{eq (1)}$$

Zeta potential. The surface zeta (ζ)-potential of pSi MPs was determined by using a disposable zeta potential cell on a Zetasizer Nano ZS (Malvern Instruments). The analysis was carried out at a temperature of 25 °C using pSi MPs dispersed in PBS buffer at pHs ranging from 5.5 to 8.5. Zeta potential was acquired from 50 runs performed in triplicate for each sample.

Thermal oxidation. A Labec horizontal tube furnace (heating rate of 20 °C/min) was used to thermally oxidise the freshly etched pSi. Samples being oxidised were situated in the middle of the furnace and the ends of the tube were closed with ceramic caps. Various oxidation temperatures (300, 400 and 500 °C) were used. All thermal oxidations commenced at room temperature and the furnace was ramped to the desired temperature before remaining at that constant temperature for 1 h. The pSi samples were allowed to slowly cool to room temperature inside the furnace. The oxidised films were cut in two smaller pieces leaving out the rim of the etched area. The pieces were then washed in ethanol and dried with nitrogen gas before being loaded with Infliximab (see loading section below).

Time-of-flight secondary ion mass spectrometry (TOF-SIMS). ToF-SIMS measurements were performed using a Physical Electronics Inc. PHI TRIFT V nanoToF instrument (Chanhassen, MN, USA) equipped with a pulsed liquid metal Au^+ primary ion gun (LMIG), operating at 30 kV. The extractor current of the ion source was maintained at 3 μA. Positive ion ToF-SIMS images (200 μm x 200 μm) were acquired on the unloaded and infliximab-loaded oxidised porous silicon macro-particles using 'unbunched' Au1 beam settings to deliver optimised spatial resolution. Positive ion mass spectra (200 μm x 200 μm) were acquired on the same surfaces using a 'bunched' Au1 beam setting for optimal mass resolution. The acquisition time for both images and spectra was 5 min each. Mass calibration of the spectra was done with CH_3^+, $C_2H_5^+$, and $C_3H_7^+$ ions. Experiments were performed a high vacuum (< 10^{-8} Torr), in static mode (i.e. below 10^{12} ions/cm^2) to minimise sample damage.

Infrared spectroscopy. Attenuated total reflectance infrared (ATR-IR) spectra were obtained using a Bruker Hyperion 1000 IR microscope operating with a Bruker Vertex 80 IR spectrometer. The IR microscope was equipped with a liquid nitrogen cooled MCT detector. ATR spectra were collected over 64 scans, with a resolution of 4 cm^{-1}, using a Ge ATR crystal. All spectra were background corrected with an unetched silicon wafer of the same type. Spectra of the pSi layers were recorded and analysed using OPUS version 7.0 software, in the range of 650 - 4000 cm^{-1}. All IR spectra are presented with absorbance normalised to the Si-O peak at approximately 1100 cm^{-1}.

Scanning electron microscopy (SEM). SEM was performed on a FEI Quanta 450 FEG environmental SEM fitted with an SSD detector, and operated at 30 keV with a spot size of 2 mm. To help facilitate the dissipation of charge build-up, samples were coated with 5 nm thick layer of Pt prior to analysis, according to our standard laboratory protocol.[12] pSi MPs were dispersed directly onto conductive aluminium stubs for analysis, and were not coated for analysis.

Loading and quantification of Infliximab. Infliximab powder was dissolved in 10 mL of sterile MilliQ water for injection, giving a drug concentration of 10 mg/mL. The solution was subsequently diluted out in PBS to achieve a working concentration of 1 mg/mL.

The antibody solution was aliquoted and stored at -80 ˚C. The loading of Infliximab (1 mg/mL, pH 7.4) into the oxidised pSi MPs was carried out using a sealed low protein binding Eppendorf tube. After loading the MPs were rinsed with PBS (pH 7.4, 15 min) to remove the weakly adsorbed antibody. The amount of protein loaded was determined from UV-Vis measurements of the supernatant before and after incubation with the pSi MPs.

Interferometric reflectance spectroscopy (IRS) of pSi films. IRS was used to monitor the effective optical thickness (EOT) of the pSi layer in time-lapse mode. The experiments were performed using an interferometer with a bifurcated fiber on a motorised stage that allowed the same sample spots to be accurately analysed. The interferometer consisted of a tungsten light source and USB2000 CCD Detector (Ocean Optics, USA). For the EOT comparison, pSi substrates were placed directly on the motorised stage and monitored in air. For degradation studies, the pSi substrates were placed in a custom-built cell, described elsewhere,[15] that allowed solutions to be flowed over the sample while monitoring the EOT in real time.

Infliximab release (using ELISA and L929 assay). Infliximab loaded pSi-MPs (15 mg) were incubated in 500 µL PBS, pH 7.2, for 2 weeks at 25 ˚C, to more closely mimic the skin surface temperature, which can vary significantly especially when wounded.[69,70] At days 1, 2, 7, 14, 21 and 28 days, samples were spun briefly to pellet the pSi and then all of the supernatant was decanted. A 500 µL aliquot of fresh PBS, pH 7.4, was added to each sample, to continue the incubation. Each aliquot was tested for the amount of antibody release via ELISA (see section, TNF-α ELISA, below) and TNF-α based bioassay (see section, TNF-α cell-based bioassay, below).

Infliximab release (using fluorimetry). Infliximab (0.1 mg/mL) was labeled with fluorescein isothiocyanate (FITC) for 4 h in a sodium carbonate buffer (100 mM, pH 9.5). After labeling the labeled protein was recovered using a Vivaspin 2 10,000 MWCO spin tube (Sartorius Stedim) according to the manufacturer's instructions. This FITC labeled protein was then added to unlabeled Infliximab at a ratio of 1:5.85 and this stock was used to load pSi MPs as outlined above. Release was then monitored on an Agilent Technologies Cary Eclipse fluorimeter fitted with a Peltier temperature control system with a PMT of 650 V and excitation and emission slit widths of 5 nm. The emission was monitored at 525 nm and the excitation was performed at 490 nm. Data was recorded in an automated kinetic mode every 8 h for 7 d. The FITC signal was calibrated against a calibration curve constructed from dilutions of the FITC labeled Infliximab stock solution.

TNF-α ELISA. The Duo TNF-α ELISA kit (R&D Systems) was used to detect non-neutralised human TNF-α as per the manufacturer's instructions. TNF-α was evaluated in post-pSi supernatant and TNF-α spiked (1 µg/mL) acute wound fluid (obtained with institutional ethics approvals Human Research Ethics Committee, The Queen Elizabeth Hospital, Lyell McEwin Hospital, Modbury Hospital (TQEH/LMH/MH) Ref#: HREC/12/TQEHLMH/107). The optical density of each well was determined immediately using a microplate reader set to 450 nm (Sunrise^{TM}, Tecan Group Ltd., Australia).

TNF-α cell-based assay. A cell-based cytotoxic bioassay based on a subclone of the murine L929 fibroblast cell line (Sigma-Aldrich, Sydney, Australia) was used.[71] Briefly, L929 cells were seeded at 2 x 10^4 cells per well in 96-well microtiter plates containing 50 µL of culture medium (Dulbecco's modified Eagle's medium containing 10% (v/v) fetal bovine serum) (Sigma-Aldrich, Sydney, Australia). The cells were incubated for 24 h before the addition of 50 µL test solution, containing from 1 mg/mL to 1 pg/mL recombinant human TNF-α (R&D Systems, Minneapolis, MN), and Infliximab released from pSi MPs to each well. Fresh Infliximab (1 to 1000 µg/mL) was added to some wells as a positive control. After a further 24 h incubation, 20 µL of 2.5 mg/mL 3-(4,5-dimethylthiazol-2-yl)-2,5-diphenyl tetrazolium bromide (MTT; Sigma-Aldrich, Sydney, Australia) and 50 µL culture medium was added per well and incubated for 4 h before solubilisation in 100 µL/well 10% (w/v) sodium dodecyl sulfate-HCl. After a final overnight incubation, the blue formazan product was measured at 570 nm on a microplate reader (Sunrise^{TM}, Tecan Group Ltd., Australia).

Statistical analysis. Statistical differences were determined using the Student's t-test or an ANOVA. For data not following a normal distribution, the Mann-Whitney U-test was performed. A P value of less than 0.05 was considered significant.

Results

Infliximab (molecular weight of 149 kDa) has a hydrodynamic radius of 5-6 nm and an isoelectric point (pI) of approximately 8.3. The radius and the pI dictate that a > 10 nm pore radius and a negative surface charge at neutral pH should be used to facilitate antibody loading and retention. When working with monoclonal antibodies, using a buffer with the correct pH and ionic strength is important.[72] As the pI of Infliximab is 8.3 working at pH 7.4 which is below this pI should keep the Infliximab positively charged and subsequently less likely to aggregate, hence, helping the protein to remain in its fully active conformation.[73] The original pSi etching conditions were adapted from previous work by Andrew *et al.*[21] However, we observed that these conditions resulted in non-homogeneous pore sizes and a microporous layer formed when etching some wafers that possess a highly doped surface layer.[74] In order to remove this microporous layer, a sacrificial etching step was applied (see Supp. Fig. 1)†.[74] After the sacrificial etching step, etching current densities from 233 to 150 mA/cm^2 were used in combination with etching times from 15 to 240 s. Interferometric reflectance spectroscopy (IRS) analysis of the effective optical thickness (EOT) from 20 locations on each film showed that the 233 mA/cm^2 etch for 20 s produced the most homogeneous surfaces with EOT variations of less than 0.20% across the scanned etched region (See Supp. Fig. 2)†.

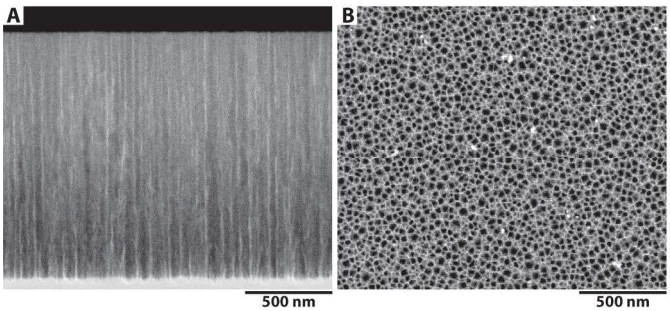

Figure 1: Scanning electron microscopy (SEM) images of (A) cross-sectional view and (B) top down view of the oxidised (400 °C) pSi film.

Scanning electron microscopy (SEM) images of the pSi surfaces etched using the optimal conditions of 233 mA cm^{-2} for 20 s and oxidised at 400 ^{o}C (Fig. 1) revealed pore sizes are approximately 22.2 ± 4.4 nm. The thickness of the porous layer, measured via SEM, was 1.39 µm and the porosity, determined by means of IRS, was 76 ± 5%.

The temperature at which the pSi film surface is oxidised controls both the extent of antibody loading (assuming that a larger difference in net charge between the pSi surface and antibody encourages more protein binding), and the rate at which the pSi will degrade in aqueous buffers. It is known from previous work that pSi functionalised at 600 °C or above will not readily degrade in aqueous solutions either *in vitro* or *in vivo*.[12] For this reason, we chose to investigate oxidation temperatures of 300, 400 and 500 °C with freshly etched pSi as a control. Figure 2 shows the average degradation curves for each oxidation temperature over a 2 h period. Combining this analysis with the pre-determined film thickness, we can estimate the expected degradation time. As anticipated, the fastest surface to degrade was the freshly etched pSi surface at a rate of 18.13 %EOT/h, resulting in complete degradation of the film in just 2.5 h (0.10 d). The time for degradation of the films oxidised at 300 °C extended to 73.8 h (3.1 d at a rate of 0.61 %EOT/h). This degradation time increased further to 201.3 h (8.4 d at 0.22 %EOT/h) for the film oxidised at 400 °C and to 790.0 h (32.91 d at 0.06 %EOT/h) for the sample after 500 °C oxidation.

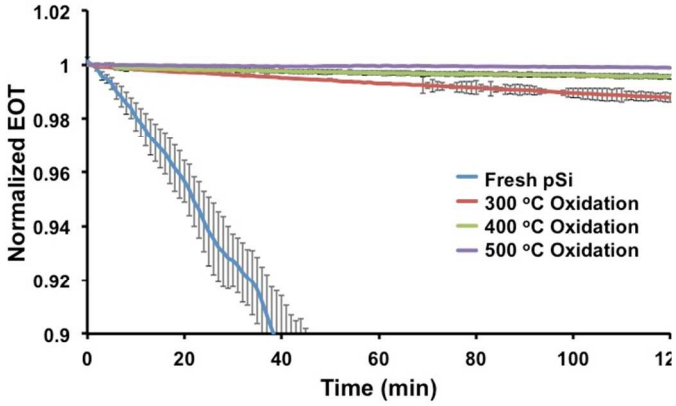

Figure 2: Degradation profiles over 120 min of freshly etched pSi films as well as pSi films oxidised at 300 °C, 400 °C and 500 °C, as determined by IRS measurements in PBS buffer at pH 7.2 at 25 °C (n=3).

The optimal etching conditions were then used to produce pSi MPs that were thicker in nature than the pSi films (Fig. 3) and could be suitable for either implantation or injection. pSi MPs were etched using the conditions adapted from those optimised for the pSi films, with an etching time of 4 min and a subsequent 30 s electropolish at 500 mA/cm^2 to lift off the film, which was then subsequently sonicated to generate particles. SEM revealed that the pSi MPs had a thickness of 23.4 ± 1.3 µm (Fig. 3A). Higher resolution SEM analysis showed an average pore diameter of 19.5 ± 8.2 nm (Fig. 3B), very similar to that of the pSi films (22.2 ± 4.4 nm, Fig. 1B). Typical particle sizes were in the range of 66.5 ± 20.9 µm. Gravimetric analysis determined the porosity of the pSi MPs to be 84.2 ± 2.0%, again very close to that of the pSi film preparations (76 ± 5%).

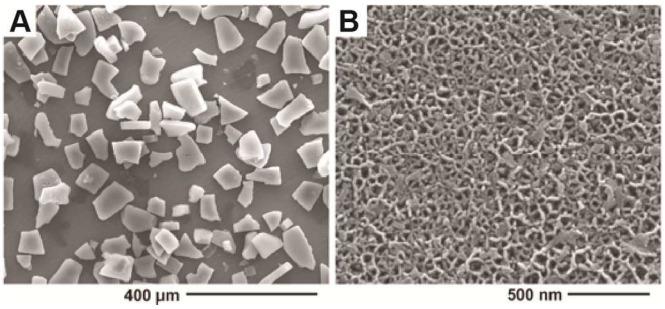

Figure 3: (A) SEM micrograph showing the size distribution of the pSi MPs and (B) higher resolution SEM micrograph showing mesopores of the pSi MPs.

Zeta potential investigations into the pSi MPs prepared with various oxidation conditions at pH 7.4 revealed that the surface was negatively charged at about -20 mV for all oxidation temperatures (Table 1).

Table 1: Zeta potential measurements of pSi MP surfaces oxidised at different temperatures in PBS at pH 7.4 (n=3).

pSi Oxidation Temperature (°C)	Zeta Potential (mV)
300	-20.3 ± 0.9
400	-19.4 ± 1.5
500	-20.3 ± 1.7

This is in line with the literature and is attributed to the presence of Si-OH on the surface.[53] Next, Infliximab binding was analysed overnight at room temperature by observing the change in zeta potential of the pSi MPs before and after the injection of Infliximab at 266 µg/mL (Fig. 4A).

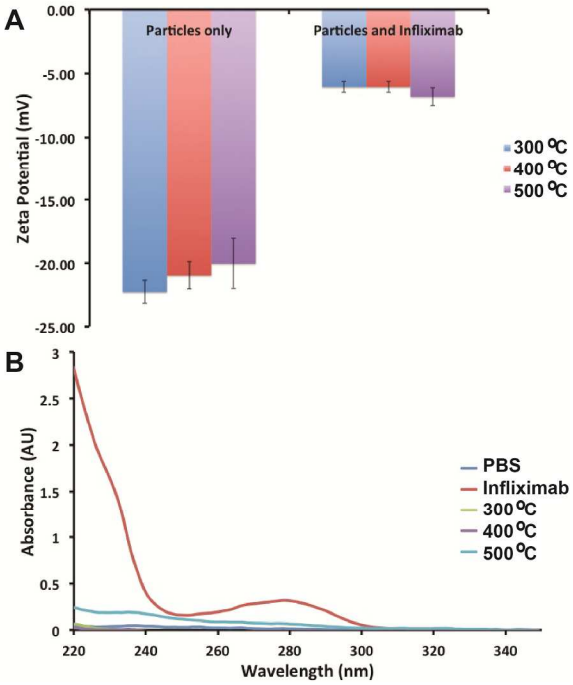

Figure 4: A) Change in zeta potential upon binding of Infliximab to pSi MPs in pH 7.4 buffer for different pSi MP oxidation conditions (300 °C, 400 °C and 500 °C) (n = 3) and B) UV-Vis monitoring of the Infliximab in supernatant during the binding experiment in panel A at pH 7.4.

It was observed that the zeta potential of the MPs after overnight incubation decreased significantly for all oxidation conditions, due to the adsorption of protein. Loading of the Infliximab into the pSi MPs during the zeta measurements was also confirmed by the UV-Vis spectroscopy of the supernatant before and after the loading experiment. The supernatant after loading showed complete removal of the protein peak at 280 nm (Fig. 4B), suggesting that the protein was completely sequestered by the pSi MPs.

Considering the degradation and zeta potential data, we chose to use 400 ^{o}C oxidised pSi MPs to perform binding Infliximab experiments since this sample was stable over several days (the desired timeframe of drug release) and was negatively charged where Infliximab at pH 7.4 is positively charged.[73]

Antibody loading experiments performed at pH 6.5 and 5.5 showed a similar trend in both zeta potential measurements and UV-Vis analysis (see Supp. Fig. 3)†, suggesting no advantage of loading at more acidic pH values. Subsequently, our typical loadings of the pSi MPs were performed with approximately 15 mg of pSi and 1 mg (at 1 mg/mL) Infliximab in PBS at 7.4. Loading values were individually assessed by UV-Vis spectrophotometry of the supernatant before and after for each particle preparation used, and were typically in the range of 0.063 ± 0.010 mg/mg similar to literature values.[52] Loadings could be further improved by the use of higher concentrations of Infliximab (see Supp. Table 1)†.

Successful loading of Infliximab was also confirmed by infrared (IR) spectroscopy. The IR in attenuated total reflection (ATR) spectra of oxidised pSi (**Fig. 5,** 400 ^{o}C oxidised pSi) showed a broad, intense peak centered at 1047 cm^{-1} attributed to the asymmetric stretching of Si-O-Si groups[75] and at 887 cm^{-1} due to Si-O bending in O-Si-O.[76] The shoulder located at approximately 1182 cm^{-1} was attributed to the stretching of surface oxide species including O-Si-O.[77-79] After loading of Infliximab, into the oxidised pSi (**Fig. 5,** 400 ^{o}C oxidised pSi with Infliximab), the spectra still showed surface peaks characteristic of oxidised pSi in addition to new peaks at 1465 cm^{-1} from the asymmetric CH_3 deformation and dual peaks at 2850 - 3000 cm^{-1} for the C-H stretching vibrations of the protein. Two prominent peaks at 1542 cm^{-1} and 1639 cm^{-1} were attributed to C–N–H bending vibrations (amide II) and C=O stretching vibrations (amide I) of the peptide bonds, respectively.[80] The 1247 cm^{-1} peak could also be ascribed to amide III of the protein,[81] while the secondary amine (N-H) stretching appeared at 3290 cm^{-1}.[80] The IR results therefore confirm the presence of Infliximab on the pSi surface. X-ray photoelectron spectroscopy (XPS) further corroborated those results (Supp. Table 2)†.

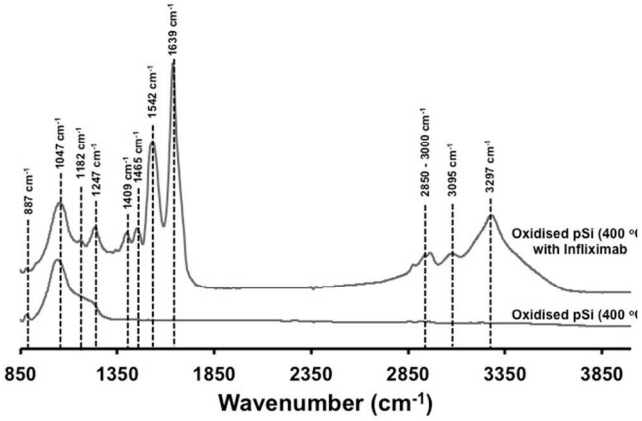

Figure 5: ATR-IR spectra of pSi film oxidised at 400 ^{o}C before and after loading of Infliximab.

To verify that Infliximab diffused completely through the oxidised pSi layer, the cross-sections of pSi films before and after Infliximab loading were imaged by time-of-flight secondary ion mass spectrometry (ToF-SIMS) to detect characteristic positive ion fragments, appearing in the mass spectra after loading Infliximab into pSi. Figure 6 shows ToF-SIMS images of the total positive ions and the total intensity of the selected positive ion fragments $C_4H_{10}N^+$ (*m/z* 72.081) and $C_5H_{12}N^+$ (*m/z* 86.096) characteristic of the amino acids valine and leucine/isoleucine, respectively[82] (see Supp Fig. 4 for ToF-SIMS mass spectra and Supp. Table 3 for Mass peak assignments)†. As expected, no signal was detected for the $C_4H_{10}N^+$ & $C_5H_{12}N^+$ positive fragments within the oxidised porous layer of the unloaded sample In contrast, both positive ion fragments were observed after Infliximab loading. The ToF-SIMS imaging also showed that the protein was present throughout the porous layer although signal intensity decreased with increasing depth. It should be noted that in order to facilitate the ToF-SIMS imaging, a very thick pSi film (80 µm) was used, much thicker than what was used for pSi MPs (**23.4** µm). Indeed, ToF-SIMS imaging of oxidised pSi MPs after loading with Infliximab showed representative positive ion fragments, $C_4H_{10}N^+$ (*m/z* 72.081) and $C_5H_{12}N^+$ (*m/z* 86.096) over across the MPs (Fig. 7). As expected, however, mapping these fragments on the unloaded oxidised pSi MPs showed a very weak intensity. While it was impractical to cross-section the oxidised pSi MPs, we expected MPs with open pores on both sides would allow antibody loading easier than pSi films.

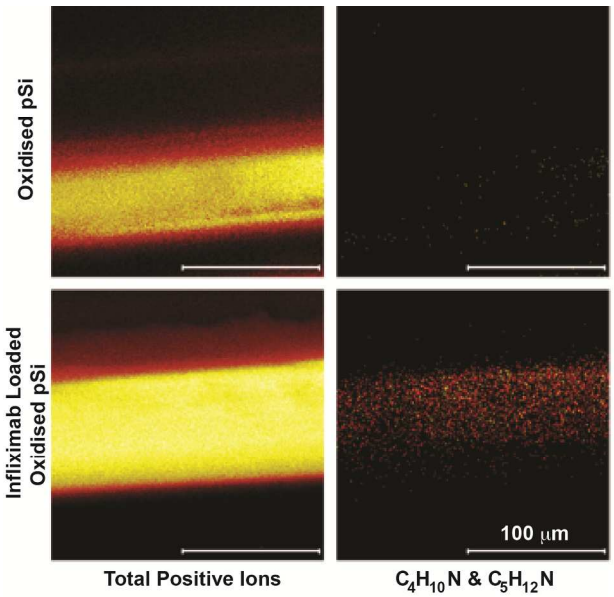

Figure 6: ToF-SIMS images (200 µm x 200 µm) for the total positive ions and for the positive ion fragments $C_4H_{10}N^+$ (*m/z* 72.081) and $C_5H_{12}N^+$ (*m/z* 86.096) characteristic of the amino acids valine and leucine/isoleucine acquired on the cross-section of oxidised pSi (400 ^{o}C) and infliximab-loaded oxidised pSi films. Scale bar on the images = 100 µm. To help aid analysis in imaging mode, pSi films were etched for 20 min to produce a pSi layer of approximately 80 µm thickness.

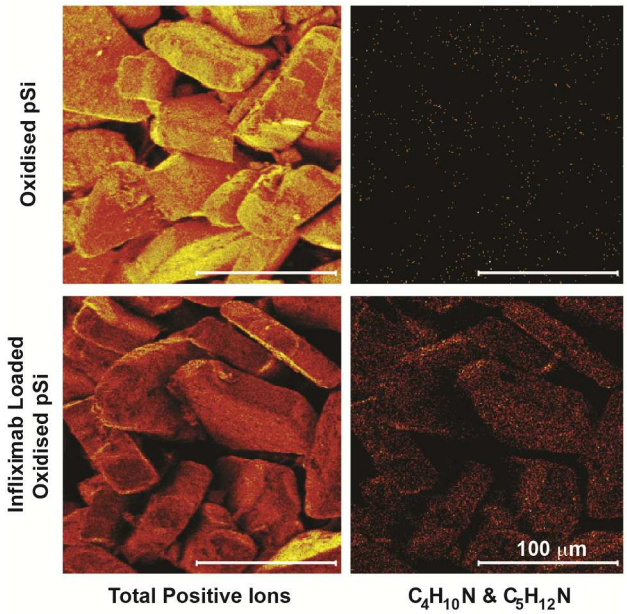

Figure 7: ToF-SIMS images (200 μm x 200 μm) for the total positive ions and for the positive ion fragments $C_4H_{10}N^+$ (*m/z* 72.081) and $C_5H_{12}N^+$ (*m/z* 86.096) characteristic of the amino acids valine and leucine/isoleucine acquired on the oxidized pSi (400 °C) and infliximab-loaded pSi MPs. Scale bar on the images = 100 μm.

To obtain the antibody release kinetics from the 400 °C pSi MPs, we followed the emission of FITC-labeled Infliximab releasing into solution via fluorimetry (Fig. 8A). The release kinetics appeared initially to show a small burst release (approx. 5.3% at 8 h) followed by a near linear release profile (R^2 = 0.976) release profile. This is desirable to maximise the therapeutic benefits of a localised drug delivery platform.[83] It was observed that the optimally loaded pSi MPs released the Infliximab at a rate of 22.56 μg of Infliximab per day. These results show that the release of Infliximab should continue for approximately 14 d (47.34% release observed at 7 d).

To test the functionality of the Infliximab released from the pSi MPs oxidised at 400 °C, we carried out a TNF-α neutralisation ELISA periodically over 14 d. Infliximab released from pSi was functional with > 90% TNF-α neutralisation observed for the day 1 and 2 samples (Fig. 8B, black bars). However, the activity of the released Infliximab diminished over time, with no effect observed past the day 7 time-point. Infliximab functionality when incubated in the absence of pSi (Fig. 8B, grey bars) (at an equivalent concentration to the amount released from pSi) was less than observed for antibody released from pSi, with no activity detected after the 2 day time-point. This indicated that the incubation of low concentrations of Infliximab in PBS at 25 °C leads to degradation, providing a limitation for the assay, but importantly provided evidence that pSi protected Infliximab from degradation prior to release.

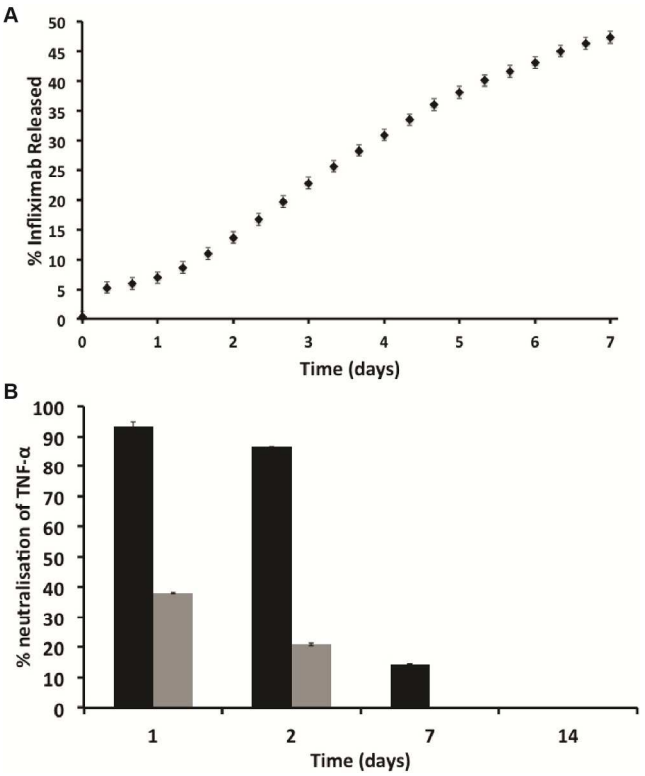

Figure 8: (A) FITC tracking of Infliximab released at 25 °C pH 7.4 from oxidised pSi MPs (400 °C) over a 7 day period. (B) ELISA detection of TNF-α. Supernatant containing Infliximab released from pSi was incubated with human TNF-α for 10 minutes at 37 °C. Non-neutralised TNF-α was then detected by ELISA. Supernatant was collected from 400 °C oxidised pSi MPs loaded with Infliximab and incubated at 25 °C over a 14 day period (black bars). Fresh Infliximab (i.e. not associated with pSi MPs) was also incubated in PBS (gray bars). Data at each time point are presented as the % inhibition of TNF-α by Infliximab. The assay was performed in triplicate and presented as mean +/- one standard deviation.

To confirm that Infliximab released from pSi MPs neutralises TNF-α, whilst showing efficacy in a cellular environment, a L929 cell bioassay was used.[71,84] Recovery of TNF-α treated L929 cells was assessed after 7, 14, 21 and 28 d of release. Recombinant TNF-α was cytotoxic to L929 cells in a dose dependent manner ($p < 0.005$) (Supp. Fig. 5)† and this cytotoxicity could subsequently be inhibited by Infliximab at ≥ 5 μg/mL (Supp. Fig. 6)†. The addition of supernatant from Infliximab-loaded pSi MPs was demonstrated to increase L929 cell viability for up to 21 d (Fig. 9A). It should be noted that the MTT assay (Fig. 9A) showed the presence of functional Infliximab in samples up to day 28, longer than could be detected by ELISA (Fig. 8B). The discrepancy may be caused by differences in the sensitivity of these two assays and variations in the strength of TNF-α/Infliximab binding due to the different buffers, pH values and incubation times required. Together, the ELISA and L929 cell bioassay was able to confirm that Infliximab released from pSi MPs remained both stable and active.

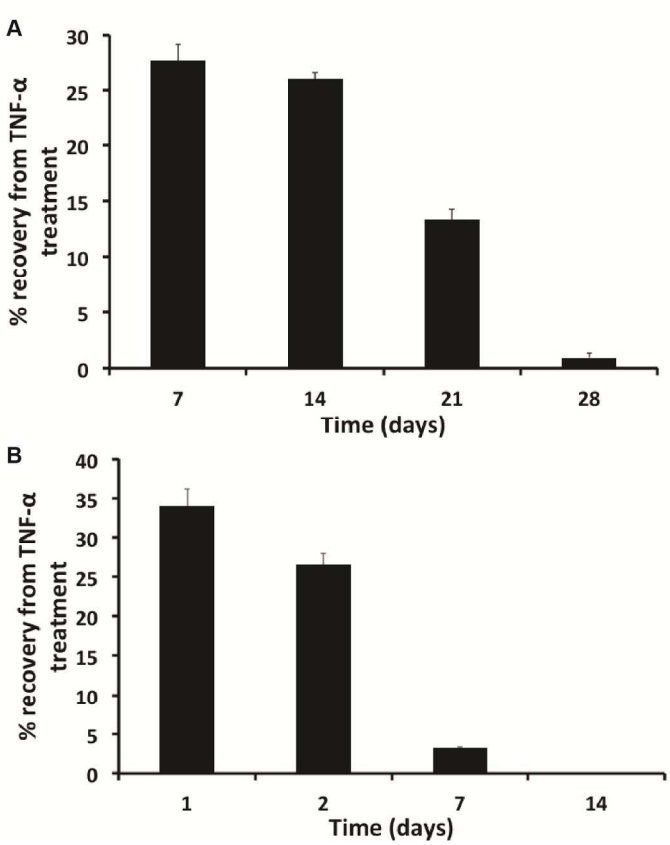

Figure 9: Recovery of TNF-α-treated L929 cell viability with Infliximab released from pSi. In panel (A), supernatant from Infliximab-loaded pSi MPs incubated at 25 ˚C in PBS was incubated with human TNF-α for 10 minutes at 37 ˚C, and then added to L929 cells. In panel (B), supernatant from Infliximab-loaded pSi MPs incubated at 25 ˚C in acute wound fluid was incubated with human TNF-α for 10 minutes at 37 ˚C, and then added to L929 cells. MTT assay was used to measure L929 cell viability using absorbance at 570 nm. Data is presented as a % recovery of L929 cells, as determined by the difference in signal between TNF-α-treated (0%) and TNF-α/Infliximab-treated (100%) cells. The assay was performed in triplicate and presented as mean +/- one standard deviation.

The applicability of this system with conditions closer to a wound environment was demonstrated via the neutralisation of TNF-α spiked into acute wound fluid (AWF) from 3 different patients (Fig. 9B). Time points of 1, 2, 7 and 14 d were analysed with the L929 cell bioassay. L929 cells could recover > 25% when exposed to supernatant incubated for 1 and 2 d. This result suggests that the pSi MPs loaded with Infliximab were able to neutralise the TNF-α in actual wound fluid samples. Additionally, the range of conditions in which Infliximab remained active was tested via the L929 assay. We observed that the L929 cells were able to respond to Infliximab treatment when high concentrations (1 mg/mL) of Infliximab were held at pH values ranging from 4.5 - 8.5 and temperatures ranging from 4 ºC to 37 ºC for up to 7 d (see Supp. Fig. 7)†. It was observed that even at the extreme pH values and temperatures approximately 70% cell recovery was observed.

The data presented here demonstrates that Infliximab is able to bind to TNF-α in a wound environment and subsequently reduces its activity. These results suggest the wide range and applicability of the delivery of Infliximab for applications ranging from wound healing to uveitis.

Conclusions

We demonstrate that oxidised pSi films and MPs have a high loading capacity for Infliximab and extend antibody release *in vitro*. In particular, we show near linear release kinetics of Infliximab from oxidized pSi MPs over 8 days. The released Infliximab was able to improve the viability of L929 cells for a 7-day period by mopping up the TNF-□ in acute wound fluid, an adequate period of time to suit a clinically application. Hence, with optimised tuning of the porous structure and its surface, the pSi films and MPs described here may represent a form of resorbable and biocompatible therapeutic carrier for the extended drug delivery requiring no surgical removal. It is envisaged that pSi MPs can be incorporated into wound dressings materials and deliver Infliximab to wound fluid in order to improve chronic wound healing. We also believe that the same Infliximab-releasing pSi MP format may be fit for the purpose of treating uveitis.

Acknowledgements

Funding from the NHMRC Project Grant 595901 is acknowledged. We thank intern students Hiten Lad and Laura Rollinger for assistance with experiments as well as Roshan Vasani for XPS analysis, Stephanie Pace for assistance in interpreting the IRS results, John Denman for assistance with acquiring ToF-SIMS spectra and Stuart McClure for performing the SEM imaging. This research was in part conducted and funded by the Australian Research Council Centre of Excellence in Convergent Bio-Nano Science and Technology (project number CE140100036).

Notes and references

[a] ARC Centre of Excellence in Convergent Bio-Nano Science and Technology, Mawson Institute, University of South Australia, Adelaide, South Australia 5001, Australia. Email: nico.voelcker@unisa.edu.au; Fax: +61 8 8302 5613; Tel: +61 8 8302 5508

[b] Mawson Institute, University of South Australia, Adelaide, South Australia 5001, Australia.

[c] Department of Ophthalmology, Flinders University, Bedford Park, South Australia, Australia

† Electronic Supplementary Information (ESI) available: Infliximab loading optimisation results, XPS analysis of Infliximab loaded pSi, L929 bioassay experimental details, ToF-SIMS data for positive Ion fragments, microporous pSi layer characterization, EOT optimization for pSi films, Zeta potential measurements and UV-Vis loadings at pH 6.5 and 5.5, ToF-SIMS mass spectra, L929 cell assay optimization and L929 assay results for various pH and temperature incubations of Infliximab. See DOI: 10.1039/b000000x/

1. S. Farajnia, V. Ahmadzadeh, A. Tanomand, K. Veisi, S. A. Khosroshahi, and L. Rahbarnia, *Immunopharmacol. Immunotoxicol.*, 2014, **36**, 297–308.
2. P. Chames, M. Van Regenmortel, E. Weiss, and D. Baty, *Br. J. Pharmacol.*, 2009, **157**, 220–233.
3. J. K. Tessmar and A. M. Göpferich, *Adv. Drug Deliv. Rev.*, 2007, **59**, 274–291.
4. H. A. Santos, *Porous silicon for biomedical applications*, Woodhead Publishing Limited, 2014.
5. L. T. Canham, *Properties of Porous Silicon*, Short Run Press, London, 2006.
6. A. Loni, in *Properties of Porous Silicon*, ed. L. Canham, Short Run Press, London, 2006.
7. S. J. P. McInnes, E. J. Szili, S. A. Al-Bataineh, J. Xu, M. E. Alf, K.

K. Gleason, R. D. Short, and N. H. Voelcker, *ACS Appl. Mater. Interfaces*, 2012, **4**, 3566–3574.
8. S. J. P. McInnes, H. Thissen, N. R. Choudhury, and N. H. Voelcker, *J. Colloid. Interface Sci.*, 2009, **332**, 336–344.
9. L. T. Canham, *Adv. Mater.*, 1995, **7**, 1033–1037.
10. L. A. R. Canham, *Phys. World*, 2001, 27–31.
11. S. D. Alvarez, A. M. Derfus, M. P. Schwartz, S. N. Bhatia, and M. J. Sailor, *Biomaterials*, 2009, **30**, 26–34.
12. S. P. Low, N. H. Voelcker, L. T. Canham, and K. A. Williams, *Biomaterials*, 2009, **30**, 2873–2880.
13. L. Cheng, E. J. Anglin, F. Cunin, D. Kim, M. J. Sailor, I. Falkenstein, A. Tammewar, and W. R. Freeman, *Br. J. Ophthalmol.*, 2008, **92**, 705–711.
14. L. M. Bimbo, M. Sarparanta, H. A. Santos, A. J. Airaksinen, E. Mäkilä, T. Laaksonen, L. Peltonen, V.-P. Lehto, J. Hirvonen, and J. Salonen, *ACS Nano*, 2010, **4**, 3023–3032.
15. E. J. Szili, A. Jane, S. P. Low, M. Sweetman, P. Macardle, S. Kumar, R. S. C. Smart, and N. H. Voelcker, *Sensor. Actuat. B: Chem.*, 2011, **160**, 341–348.
16. M. J. Sailor and J.-H. Park, *Adv. Mater.*, 2012, **24**, 3779–3802.
17. F. S. H. Krismastuti, S. Pace, E. Melville, A. J. Cowin, T. R. Dargaville, and N. H. Voelcker, *Aust. J. Chem.*, 2013, **66**, 1428–1434.
18. S. Pace, R. B. Vasani, F. Cunin, and N. H. Voelcker, *New J. Chem.*, 2012, **37**, 228–235.
19. A. M. Rossi, L. Wang, V. Reipa, and T. E. Murphy, *Biosens. Bioelectron.*, 2007, **23**, 741–745.
20. J. Salonen, L. Laitinen, A. Kaukonen, J. Tuura, M. Bjorkqvist, T. Heikkila, K. Vaha-Heikkila, J. Hirvonen, and V.-P. Lehto, *J. Control. Release*, 2005, **108**, 362–374.
21. J. S. Andrew, E. J. Anglin, E. C. Wu, M. Y. Chen, L. Cheng, W. R. Freeman, and M. J. Sailor, *Adv. Funct. Mater.*, 2010, **20**, 4168–4174.
22. J. Rytkönen, P. Arukuusk, W. Xu, K. Kurrikoff, Ü. Langel, V.-P. Lehto, and A. Närvänen, *Mol. Pharm.*, 2014, **11**, 382–390.
23. Z. P. Xu, Q. H. Zeng, G. Q. Lu, and A. B. Yu, *New J. Chem.*, 2003, **27**, 1027–1040.
24. Y.-L. Khung, S. D. Graney, and N. H. Voelcker, *Biotechnol. Progress*, 2008, **22**, 1388–1393.
25. A. Janshoff, K.-P. S. Dancil, C. Steinem, D. P. Greiner, V. S. Y. Lin, C. Gurtner, K. Motesharei, M. J. Sailor, and M. R. Ghadiri, *J. Am. Chem. Soc.*, 1998, **120**, 12108–12116.
26. M. P. Stewart and J. M. Buriak, *Adv. Mater.*, 2000, **12**, 859–869.
27. J. Salonen and V.-P. Lehto, *Chem. Eng. J.*, 2008, **137**, 162–172.
28. S. Low, K. Williams, L. Canham, and N. H. Voelcker, *Biomaterials*, 2006, **27**, 4538–4546.
29. L. A. Perelman, C. Pacholski, Y. Y. Li, M. S. VanNieuwenhze, and M. J. Sailor, *Nanomed.*, 2008, **3**, 31–43.
30. S. Bayliss, L. Buckberry, P. Harris, and M. Tobin, *J. Porous Mater.*, 1999, **7**, 191–195.
31. Y. L. Khung, G. Barritt, and N. H. Voelcker, *Exp. Cell Res.*, 2008, **314**, 789–800.
32. S. Kashanian, F. Harding, Y. Irani, S. Klebe, K. Marshall, A. Loni, L. Canham, D. Fan, K. A. Williams, N. H. Voelcker, and J. L. Coffer, *Acta Biomaterialia*, 2010, **6**, 3566–3572.
33. J. Chhablani, A. Nieto, H. Hou, E. C. Wu, W. R. Freeman, M. J. Sailor, and L. Cheng, *Invest. Ophthalmol. Vis. Sci.*, 2013, **54**, 1268–1279.
34. K. Zhang, S. L. Loong, C. Connor, S. W. Yu, T. SY, R. T. Ng, K. M. Lee, L. T. Canham, and P. K. Chow, *Clin. Cancer Res.*, 2005, **11**, 7532–7537.
35. J. R. Dorvee, A. M. Derfus, S. N. Bhatia, and M. J. Sailor, *Nat. Mater.*, 2004, **3**, 896–899.
36. J. Link and M. Sailor, *PNAS*, 2003, **100**, 10607–10610.
37. J. C. Thomas, C. Pacholski, and M. J. Sailor, *Lab Chip*, 2006, **6**, 782–787.
38. E. C. Wu, J.-H. Park, J. Park, E. Segal, F. Cunin, and M. J. Sailor, *ACS Nano*, 2008, **2**, 2401–2409.
39. M. G. Donato, M. A. Monaca, G. Faggio, L. De Stefano, P. H. Jones, P. G. Gucciardi, and O. M. Marago, *Nanotechnology*, 2011, **22**, 505704–1–505704–8.
40. K. I. Hartmann, A. Nieto, E. C. Wu, W. R. Freeman, J. S. Kim, J. Chhablani, M. J. Sailor, and L. Cheng, *J. Ocul. Pharmacol. Ther.*, 2013, **29**, 493–500.
41. H. Hou, A. Nieto, F. Ma, W. R. Freeman, M. J. Sailor, and L. Cheng, *J. Control. Release*, 2014, **178**, 46–54.
42. K. Nan, F. Ma, H. Hou, W. R. Freeman, M. J. Sailor, and L. Cheng, *Acta Biomaterialia*, 2014, **10**, 3505–3512.
43. A. Nieto, H. Hou, M. J. Sailor, W. R. Freeman, and L. Cheng, *Exp. Eye Res.*, 2013, **116**, 161–168.
44. E. Secret, K. Smith, V. Dubljevic, E. Moore, P. Macardle, B. Delalat, M.-L. Rogers, T. G. Johns, J.-O. Durand, F. Cunin, and N. H. Voelcker, *Adv. Healthcare Mater.*, 2013, **2**, 718–727.
45. B. Guan, A. Magenau, S. Ciampi, K. Gaus, P. J. Reece, and J. J. Gooding, *Bioconjug. Chem.*, 2014, **25**, 1282–1289.
46. C. Pacholski, M. Sartor, M. J. Sailor, F. Cunin, and G. M. Miskelly, *J. Am. Chem. Soc.*, 2005, **127**, 11636–11645.
47. N. Naveas, V. T. Costa, D. Gallach, J. Hernandez-Montelongo, R. J. M. Palma, J. P. Garcia-Ruiz, and M. Manso-Silván, *Sci. Technol. Adv. Mater.*, 2012, **13**, 045009.
48. L. R. Clements, P.-Y. Wang, F. Harding, W.-B. Tsai, H. Thissen, and N. H. Voelcker, *Phys. Stat. Sol. (a)*, 2010, **208**, 1440–1445.
49. A. Schlossbauer, D. Schaffert, J. Kecht, E. Wagner, and T. Bein, *J. Am. Chem. Soc.*, 2008, **130**, 12558–12559.
50. A. Foraker, R. Walcazak, M. Cohen, T. Boiarski, C. Grove, and P. Swaan, *Pharm. Res.*, 2003, **20**, 110–116.
51. J. Wu and M. J. Sailor, *Adv. Funct. Mater.*, 2009, **19**, 733–741.
52. C. A. Prestidge, T. J. Barnes, A. Mierczynska-Vasilev, W. Skinner, F. Peddie, and C. Barnett, *Phys. Stat. Sol. (a)*, 2007, **204**, 3361–3366.
53. K. L. Jarvis, T. J. Barnes, and C. A. Prestidge, *Langmuir*, 2010, **26**, 14316–14322.
54. K. L. Jarvis, T. J. Barnes, and C. A. Prestidge, *Langmuir*, 2008, **24**, 14222–14226.
55. F. I. Scott and M. T. Osterman, *Clin. Colon Rectal Surg.*, 2013, **26**, 67–74.
56. X. Ma and S. Xu, *Biomed. Rep.*, 2012, **1**, 177–184.
57. L. H. Kircik and J. Q. Del Rosso, *J. Drugs Dermatol.*, 2009, **8**, 546–559.
58. E. O. Demirsoy, R. Kiran, S. Salman, C. Caglayan, A. S. Akturk, D. Bayramgurler, and N. Bilen, *J. Drugs Dermatol.*, 2013, **12**, 1039–1043.
59. D. J. Gracie and A. C. Ford, *Minerva Gastrenterol. Dietol.*, 2012, **58**, 87–99.
60. S. J. Mehta, A. R. Silver, and J. O. Lindsay, *Aliment. Pharmacol. Ther.*, 2013, **38**, 77–97.
61. Y. J. Tai and R. Kelly, *Australas. J. Dermatol.*, 2005, **46**, 161–164.
62. M. A. Murphy, W. P. Joyce, C. Condron, and D. Bouchier-Hayes, *Eur. J. Vasc. Endovasc.*, 2002, **23**, 349–352.
63. G. Ferrari, F. Bignami, C. Giacomini, S. Franchini, and P. Rama, *Invest. Ophthalmol. Vis. Sci.*, 2013, **54**, 1680–1688.
64. J. Said, C. C. Dodoo, M. Walker, D. Parsons, P. Stapleton, A. E. Beezer, and S. Gaisford, *Int. J. Pharm.*, 2014, **462**, 123–128.
65. J. R. Smith, R. D. Smith, G. N. Holland, D. A. Jabs, M. R. Robinson, S. M. Whitcup, and J. T. Rosebaum, *Arthrit. Care Res.*, 2001, **45**, 252–257.
66. M. De Bandt, J. Sibilia, X. Le Loët, S. Prouzeau, B. Fautrel, C. Marcelli, E. Boucquillard, J. Siame, and X. Mariette, *Arthrit. Res. Ther.*, 2005, **7**, R545–R551.
67. M. Streit, Z. Beleznay, and L. R. Braathen, *Int. Wound J.*, 2006, **3**, 171–179.
68. W. Armarego and D. Perrin, *Purification of laboratory chemicals, fourth edition*, Butterworth-Heinemann, 1996.
69. W. McGuiness, E. Vella, and D. Harrison, *J. Wound Care*, 2004, **13**, 383–385.
70. P. Abraham, M. Bourgeau, M. Camo, A. Humeau-Heurtier, S. Durand, P. Rousseau, and G. Mahe, *Microvasc. Res.*, 2013, **88**, 56–60.
71. B. J. Sugarman, B. B. Aggarwal, P. E. Hass, I. S. Figari, M. A. Palladino Jr, and H. M. Shepard, *Science*, 1985, **230**, 943–945.
72. P. Kheddo, M. Tracka, J. Armer, R. J. Dearman, S. Uddin, C. F. van der Walle, and A. P. Golovanov, *Int. J. Pharm.*, 2014, **473**, 126–133.
73. R. Chaudhuri, Y. Cheng, C. R. Middaugh, and D. B. Volkin, *AAPS J.*, 2013, **16**, 48–64.
74. B. Sciacca, E. Secret, S. Pace, P. Gonzalez, F. Geobaldo, F.

Quignard, and F. Cunin, *J. Mater. Chem.*, 2011, **21**, 2294–2302.
75. S. A. Mirji, S. B. Halligudi, N. Mathew, V. Ravia, N. E. Jacob, and K. R. Patil, *Colloids Surf. A: Physicochem. Eng. Aspects*, 2006, **287**, 51–58.
76. O. Bisi, S. Ossicini, and L. Pavesi, *Surf. Sci. Rep.*, 2000, **38**, 1–126.
77. K. L. Pong, S.-C. Chen, and K. W. Cheah, *Solid State Commun.*, 1996, **99**, 887–890.
78. F. X. Qiu, P. P. Li, and D. Y. Yang, *eXPRESS Polym. Lett.*, 2007, **1**, 150–156.
79. E. Kondoha, T. Asano, A. Nakashima, and M. Komatu, *J. Vac. Sci. Technol. B*, 2000, **18**, 1276–1280.
80. M. E. Alf, T. A. Hatton, and K. K. Gleason, *Thin Solid Films*, 2011, 1–3.
81. D. Zhao, G. Liu, D. Song, J.-H. Liu, Y. Zhou, J. Ou, and S. Sun, eds. G. von Bally and Q. Luo, SPIE, 2006, vol. 6026, pp. 60260H–60260H–7.
82. H. E. Canavan, D. J. Graham, X. Cheng, B. D. Ratner, and D. G. Castner, *Langmuir*, 2007, **23**, 50–56.
83. S. J. P. McInnes and N. H. Voelcker, *Future Med. Chem.*, 2009, **1**, 1051–1074.
84. A. J. Cowin, N. Hatzirodos, J. Rigden, R. Fitridge, and D. A. Belford, *Wound Repair Regen.*, 2006, **14**, 421–426.

